AIP Journal of Applied Physics

Determination of thermal and optical properties of ion implanted polyetheretherketone films by photothermal spectroscopies

J. E. de Albuquerque, E. Tavenner, M. Curry, R. E. Giedd, and P. Meredith

Citation: Journal of Applied Physics **101**, 054506 (2007); doi: 10.1063/1.2436465
View online: http://dx.doi.org/10.1063/1.2436465
View Table of Contents: http://scitation.aip.org/content/aip/journal/jap/101/5?ver=pdfcov
Published by the AIP Publishing

Determination of thermal and optical properties of ion implanted polyetheretherketone films by photothermal spectroscopies

J. E. de Albuquerque[a)]
Departamento de Física, Universidade Federal de Viçosa, Viçosa, 36571-000 Minas Gerais, Brazil

E. Tavenner
School of Physical Sciences, University of Queensland, Brisbane, Queensland 4072, Australia

M. Curry and R. E. Giedd
Department of Physics, Astronomy & Material Science, Missouri State University, Springfield, Missouri 65804

P. Meredith[b)]
Soft Condensed Matter Physics Group, Department of Physics, University of Queensland, Brisbane, Queensland 4072, Australia

(Received 3 September 2006; accepted 13 December 2006; published online 5 March 2007)

Photothermal spectroscopies, photopyroelectric spectroscopy and photoacoustic spectroscopy (PAS), were used to study the thermal and optical properties of untreated and N^+ ion implanted polyetheretherketone (PEEK) films. The photopyroelectric (PPE) intensity signal and its phase were independently measured as a function of wavelength and chopping frequency in the saturation part of the PPE spectrum. Equations for both the intensity and the phase of the PPE signal were used to fit the experimental results. From these fits we obtained the thermal diffusivity coefficient, the thermal conductivity, and the specific heat of the samples, as well as a value for the condensed phase optical gap. Additionally, using PAS we carried out a quantitative depth profile analysis of the optical properties of the ion implanted PEEK films. Since the thermal diffusion length varies inversely with the square root of chopping modulation frequency, at high chopping frequencies surface information is obtained. At low chopping frequencies information concerning the properties of the bulk is obtained. The overall objectives of this study are to understand and quantify how ion implantation affects the thermal and optical properties of the polymer, particularly within the implant region. We find that significant changes do occur, and our results have implications for the use of ion implantation to create plastic electronic and sensor devices. © *2007 American Institute of Physics*. [DOI: 10.1063/1.2436465]

I. INTRODUCTION

Polyetheretherketone (PEEK) (see Fig. 1 for monomer structure) is a high performance thermoplastic with high temperature resistance (can be maintained at temperatures of ~460 °C), high chemical resistance, good radiation resistance, low flammability, and good mechanical properties. PEEK products can come in an opaque, crystalline form or in a transparent, amorphous, flexible thin film. PEEK is used in applications which experience highly demanding environments.[1] PEEK products are produced by a high temperature, high pressure molding process, and the polymer can survive recasting, and hence, be recycled. Ion treatment of PEEK has been shown to induce chemical, mechanical, and electrical changes, and ion implanted PEEK has been used to create devices such as infrared bolometers.[2–9] It has also been suggested that ion implantation of PEEK and other such polymers could be used to create low cost plastic circuitry and circuit elements.[2]

Photothermal spectroscopic (PTS) techniques have been extensively and successfully applied to solid state materials to obtain their thermal and optical parameters.[10–13] Among the PTS techniques, photoacoustic spectroscopy (PAS),[14] which is the most traditional one, and the more recent photopyroelectric spectroscopy[15] (PPES) have been used for studying thermal and optical properties of polymeric films and semiconductors.[16–24] In these techniques a pulsed light beam is absorbed in a solid sample and the converted heat diffuses into the bulk structure; the sample expansion, or the temperature gradient, is then detected by an appropriate sensor system. The detected signal depends on the optical and thermal properties of the sample: the optical absorption coefficient $\beta(\lambda)$ (λ being the light wavelength), the nonradiative conversion efficiency $\eta(\lambda)$, the thermal conductivity k, and the thermal diffusivity coefficient α. The signal also depends on experimental control parameters such as the chopping frequency f of the incident light beam. Of the various physical parameters which can be measured, the thermal diffusivity is particularly important because it allows one to obtain the thermal conductivity and specific heat. When the thermal conductivity is known, information can be obtained regarding the heat transfer process by phonons and by carriers (electrons or holes). In this current study, we used samples of PEEK as self-supported films. Our objective was

[a)]Author to whom correspondence should be addressed; electronic mail: jeduardo@ufv.br
[b)]Electronic mail: meredith@physics.uq.edu.au

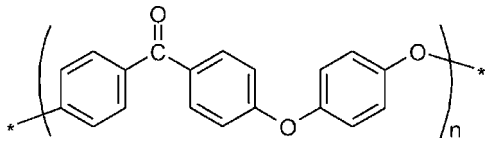

FIG. 1. PEEK monomer structure.

to study how the ion implantation process changes the thermal and optical parameters of the PEEK samples. In particular, we wished to probe and understand changes that occur within the implantation region (~ the top 100 nm of the surface). For this purpose, we used PPES to obtain the thermal diffusivity coefficient of PEEK films, and utilizing these data, we used PAS for a quantitative depth profile study by wavelength scanning in various light modulation regimes. Our work is motivated by a desire to understand the physical and chemical consequences of ion implantation in polymers with a view to creating low cost plastic circuitry, circuit elements, and sensors.

II. MANDELIS-ZVER THEORETICAL MODEL (PPES)

The photopyroelectric (PPE) spectrometer used in our experiments is schematically shown in Fig. 2. It comprises an optical part (light source, monochromator, and chopper), the custom-made pyroelectric chamber, and the measuring system. The measuring system is composed of a lock-in amplifier, locked at the chopper frequency, connected to a microcomputer that stores the data and controls the experiment. The mechanical slotted wheel chopper modulates the incident light whose intensity obeys the expression[14–16,19,23]

$$I = \frac{I_o}{2}[1 + \cos(\omega t)], \tag{1}$$

where I_o is the amplitude of the beam intensity and ω $(=2\pi f)$ is the angular chopping frequency. The absorption of this modulated pulsed light gives rise to a periodic heating of the sample owing to nonradiative relaxation of excited states. The nonradiative conversion efficiency $\eta(\lambda)$ is considered near unity, since luminescence effects in PEEK have very low efficiency over the wavelength used in this study. The generated heat is detected by a pyroelectric detector which is in direct contact with the sample.

The detected signal $V(\omega,t)$ is proportional to the pyroelectric coefficient p of the detector and to the temperature distribution along the detector thickness:[15,16,18,19,22,23]

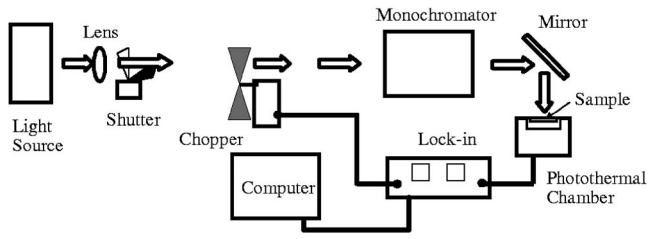

FIG. 2. Schematic of the experimental setup used for photothermal spectroscopy measurements of PEEK samples. Illumination and acquisition were synchronized using a lock-in amplification arrangement.

$$V(\omega,t) = \left[\frac{p}{K\varepsilon_0}\int_{L_P} T_P(\omega,x)dx\right]e^{i\omega t}, \tag{2}$$

where L_p is the detector thickness, $T_p(\omega,x)$ the temperature field in the bulk of the detector, K the relative dielectric constant of the material, $i=\sqrt{-1}$, and ε_o the vacuum dielectric permittivity. The heat propagation across the whole chamber is governed by heat diffusion equations of each medium coupled via boundary conditions at the interfaces ($T_a=T_b$ and $k_a dT_a/dx=k_b dT_b/dx$, a and b representing consecutive media), as established by Mandelis and Zver.[15] The signal $V(\omega,t)$ obtained by integrating the diffusion equations is normalized by the ratio $V(\omega,t)/V_R$, where V_R is the signal measured directly over the detector painted with a very thin layer of a black ink. In this latter case the detector is considered thermally thick and optically opaque, i.e., $\mu_p < L_p$ and $\beta_p^{-1} < L_p$, where $\mu_p=(\alpha_p/\pi f)^{1/2}$ is the thermal diffusion length of the detector and β_p^{-1} is its optical absorption length. Thus, $\exp(\pm\sigma_R L_R)\approx 1$, $|r_R| \gg 1$, and $\eta_R \approx 1$, where $r_n=\beta_n/\sigma_n$ and $\sigma_n=(1+i)a_n$, with $a_n=(\pi f/\alpha_n)^{1/2}$ $(n=g,s,p$; that is, $g=$gas, $s=$sample, and $p=$pyroelectric). Then, the normalized voltage signal results in[16,19,23,24]

$$\begin{aligned} V_n(\beta_S,\omega) &= \left\{\left(\frac{\eta_S r_S}{r_S^2-1}\right)\{2(b_{gs}+r_s) - [(r_s+1)(b_{gs}+1)e^{\sigma_S L_S} \right. \\ &\quad - (r_s-1)(b_{gs}-1)e^{-\sigma_S L_S}]e^{-\beta_S L_S}\} \\ &\quad \left. + [(b_{gs}+1)e^{\sigma_S L_S} - (b_{gs}-1)e^{-\sigma_S L_S}]e^{-\beta_S L_S}\right\} \\ &\quad \times\left[\frac{b_{gs}+b_{ps}}{(b_{gs}+1)(b_{ps}+1)e^{\sigma_S L_S} - (b_{gs}-1)(b_{ps}-1)e^{-\sigma_S L_S}}\right], \end{aligned} \tag{3}$$

where $b_{nm}=k_n a_n/k_m a_m$ and L_S is the sample thickness. Equation (3) is a complex function of the thermal, optical, and geometrical parameters of the system, and it governs our results since we worked at chopper frequencies above the minimum required for its validation ($\mu_p < L_p$, which means frequencies above 9.8 Hz). Assuming the case where the sample is in an optically opaque condition, that is, in the saturated region of the spectra, then the normalized voltage signal results in[16,18,22]

$$V_n(\omega) = 2\eta_S\left[\frac{(b_{gs}+b_{ps})}{(b_{gs}+1)(b_{ps}+1)e^{\sigma_S L_S} - (b_{gs}-1)(b_{ps}-1)e^{-\sigma_S L_S}}\right] \tag{4}$$

and the corresponding phase equation[16,22]

$$F_n(\omega) = -\arctan\left[\frac{(b_{gs}b_{ps}+1)\cosh(a_sL_s)+(b_{gs}+b_{ps})\sinh(a_sL_s)}{(b_{gs}+b_{ps})\cosh(a_sL_s)+(b_{gs}b_{ps}+1)\sinh(a_sL_s)}\tan(a_sL_s)\right]. \quad (5)$$

Equations (4) and (5) are complex functions and are used to obtain the thermal parameters: thermal diffusivity α and thermal conductivity k. Then, utilizing the relation $k=\rho c\alpha$, where ρ is the mass density and c is the specific heat, valid for a stationary state, we can obtain the specific heat of the sample c_s.[16,18,22]

III. ROSENCWAIG-GERSHO THEORETICAL MODEL (PAS)

In the case of the PAS, the heat propagation across the whole chamber is governed by heat diffusion equations of each medium coupled via the boundary conditions at the interfaces ($T_a=T_b$ and $k_a dT_a/dx=k_b dT_b/dx$), as established by the Rosencwaig-Gersho theory,[14] whose normalized photoacoustic signal (S_n) produced by the microphone (the pressure variation of the gas) is[17,18]

$$S_n = \frac{\eta_s r_s b_{bs}}{r_s^2-1}[(r_s-1)(b_{bs}+1)e^{\sigma_S L_S} - (r_s+1)(b_{bs}-1)e^{-\sigma_S L_S}+2(b_{bs}-r_s)e^{-\beta_S L_S}] \times \frac{1}{[(b_{gs}+1)(b_{bs}+1)e^{\sigma_S L_S}-(b_{gs}-1)(b_{bs}-1)e^{-\sigma_S L_S}]}, \quad (6)$$

where $r_s=\beta_s/\sigma_s$, $\sigma_s=(1+i)a_s$ with $a_s=(\pi f/\alpha_s)^{1/2}$, $b_{nm}=k_n a_n/k_m a_m$ ($n=g,s,b$; that is, g=gas, s=sample, and b=backing), and L_S is the sample thickness. This equation is a complex function of the optical, thermal, and geometrical parameters of the system, and it governs our results for all chopper frequencies. As the thermal diffusion length is the reciprocal value of a_s, i.e.,

$$\mu_S = \sqrt{\frac{\alpha_S}{\pi f}}, \quad (7)$$

it varies inversely as the square root of chopper frequency. Hence we can conduct a depth profile analysis by performing wavelength scans at various chopper modulation frequencies.

IV. EXPERIMENTAL METHODOLOGY

A. The photothermal spectrometer

The photothermal spectrometer used in our experiments is schematically shown in Fig. 2. The monochromator was a Sciencetech model 9055F. Note that an optical cable can be connected to the photothermal chamber, substituting for the mirror, or the chamber can be attached directly onto the exit slit of the monochromator. The measuring system was composed of a Stanford Research System SR 530 lock-in amplifier locked at the chopper frequency. Data were acquired automatically, and the system was controlled by a computer via a general purpose interface bus. The mechanical slotted wheel chopper (Stanford Research System SR 540) modulated the incident light. The power source was a 450 W xenon lamp (Thermo Oriel).

B. Photopyroelectric and photoacoustic cells

The PPE and photoacoustic (PA) chambers were designed and constructed at The Federal University of Viçosa. The PPE cell was set up with a silica window above the PEEK samples. The pyroelectric detector was a 52 μm thick β-polyvinylidene difluoride (PVDF) film with Ni–Cu electrodes evaporated on both surfaces for electrical contacts, one of which was painted with a very thin layer of black ink and was in direct contact with the sample. The values for the thermal and electrical parameters of PVDF at room temperature (as provided by the manufacturer) are 3.0×10^{-5} C/m^2 K for the pyroelectric coefficient, 12 for the relative dielectric constant, 5.4×10^{-8} m^2/s for the thermal diffusivity, and 0.13 W/m K for the thermal conductivity. The heat generated by the absorption of the chopped probe produces the voltage in the pyroelectric detector, and the signal is measured by the lock-in amplifier.

The PA cell was set up with a silica front window and with a silica plate as the backing material. We used a commercially available microphone for the PA detection. It presented a resonance region for frequencies between ~1500 and 3000 Hz with a resonance peak at 2500 Hz. This behavior was verified by a chopper frequency scanning spectrum using a blackbody sample in the chamber and a 7 mW red He:Ne laser as a power source.

C. UV–Vis measurements

UV–Vis spectral measurements were carried out with a Perkin Elmer Lambda 40 spectrometer fitted with a Labsphere RSA-PE-20 integrating sphere accessory. Total transmission spectra were acquired using a diffuse reflection standard mounted on the reflectance port at an angle of 8° and with the sample mounted on the transmittance port with the treated side towards the illumination source. Total reflection spectra were acquired by mounting samples on the reflectance port at an angle of 8° with the treated side towards the illumination source. Specular reflection reference scans were obtained with a front surface aluminum mirror mounted on the reflectance port. Absorption spectra were calculated from the transmission and reflection spectra using % absorption =100%−(% transmission+% reflection).

D. Sample preparation

Samples were prepared from PEEK films obtained from the Goodfellow Corporation. These films have an amorphous structure and are transparent with a slight amber color. The untreated PEEK film was cleaned with methanol with no

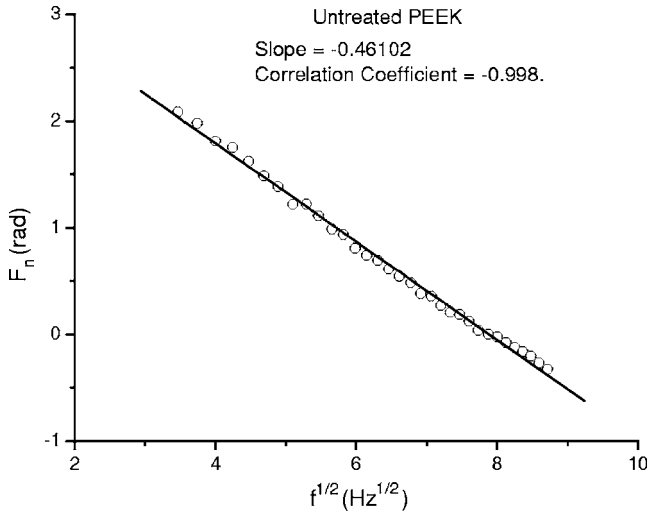

FIG. 3. Experimental points (dots) and line of best fit for the PPE normalized phase of the untreated PEEK film as a function of the chopping frequency of the input Xe lamp irradiation using the monochromator fixed at 340 nm.

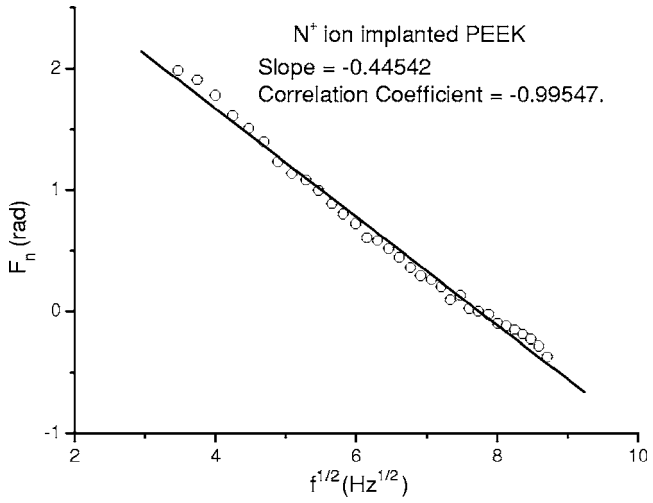

FIG. 4. Experimental points (dots) and line of best fit for the PPE normalized phase of the N^+ implanted PEEK film as a function of the chopping frequency of the input Xe lamp irradiation using the monochromator fixed at 340 nm.

further preparation. The nitrogen ion implanted PEEK film was cleaned with methanol and then attached onto glass microscope slides with double sided sticky tape for the purpose of mounting in the ion implanter. The sample was then implanted with 50 keV N^+ ions to a dose of 1×10^{16} ions/cm^2 by an IBM Taconic high current ion implanter located at the Missouri State University.

Samples were cut into rectangles of $\sim 0.8 \times 1.0$ cm^2. For PPES, the treated surface of N^+ implanted PEEK was placed in direct contact with the PVDF detector, so that the probe was incident on the untreated surface, and also measurements were made in the opposite geometry. We utilized a very thin layer of vacuum grease between the PVDF sensor and the samples in order to minimize the contact thermal impedance. From run to run and from sample to sample, we always used the vacuum grease, so the thermal impedance was always the same. For PAS, the sample was configured such that the probe was incident on the ion implanted side. In this geometry, lower chopping frequencies produce information from deeper within the sample.

V. RESULTS AND DISCUSSION

A. Determination of thermal diffusivity of PEEK films

Figures 3 and 4 show the normalized phase $F_n(f)$ as function of the square root of the chopping frequency for the untreated and N^+ implanted PEEK films, respectively. For N^+ implanted PEEK film, the measurements were done with the treated face in contact with the pyroelectric sensor. The thickness of these samples was 113 μm. The data were recorded in the saturated region of the PPE spectra, for the case where the detector is thermally thick (>12 Hz). The power source was the Xe lamp passing through the monochromator fixed at 340 nm. The experimental points for the normalized phase obey a linear dependence on the square root of the frequency for frequencies below ~80 Hz (see Figs. 3 and 4). This means that the fractional term that precedes $\tan(a_s L_s)$ in Eq. (5) is approximately unity in this frequency range. In fact, this fraction differs from unity by less than 4.2% in that frequency range when we consider appropriate values for thermal conductivity and diffusivity coefficients. This permits us to approximate Eq. (5) to the simple relation $F_n \cong -a_S L_S$. As such, the thermal diffusivity α_S is directly obtained from the slope of the fitting curve F_n vs $f^{1/2}$ (the continuous line of Figs. 3 and 4), using the relation $a_S = (\pi f/\alpha_S)^{1/2}$. Values obtained from this analysis are shown in Table I.

The α_S values of Table I were then used for the $V_n(f)$ fitting utilizing Eq. (4), and the thermal conductivity k_S became the single adjusted parameter of the results shown in Figs. 5 and 6 for the untreated and N^+ implanted PEEK films. We have to emphasize that the thermal diffusivity for ion implanted PEEK in our case is an average value of the bulk (unimplanted) and surface (implanted), because our samples can be thought of as a monolayer system amended

TABLE I. Physical parameters of untreated PEEK and N^+ ion implanted PEEK.

	Untreated PEEK	N^+ ion implanted PEEK (untreated face in contact with PVDF)	N^+ ion implanted PEEK (treated face in contact with PVDF)
L_s (μm)	113±5	113±5	113±5
α_s (m^2/s)	$(1.9\pm0.2)\times10^{-7}$	$(2.0\pm0.2)\times10^{-7}$	$(2.5\pm0.2)\times10^{-7}$
k_s (W/m K)	0.32±0.1	0.55±0.03	0.65±0.04
c_S (J/kg K)	$(1.3\pm0.1)\times10^3$	$(2.1\pm0.2)\times10^3$	$(2.0\pm0.2)\times10^3$

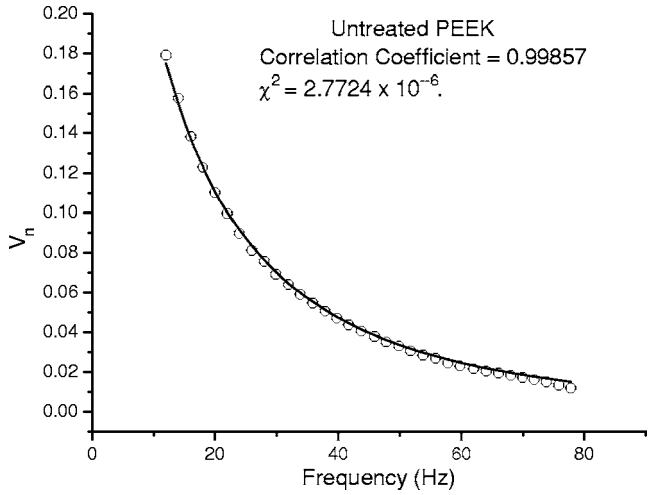

FIG. 5. Experimental points (dots) and line of best fit [Eq. (4)] for the PPE normalized voltage of the untreated PEEK film as a function of the chopping frequency of the input Xe lamp irradiation using the monochromator fixed at 340 nm.

by a very thin layer of implanted region. Note that there is a difference in the parameters obtained for the N^+ ion implanted PEEK film with the treated face in contact or not in contact with the PVDF detector. Table I shows these differences. This is likely due to the asymmetry in the system (the implant region is much thinner than the film thickness). The specific heat of the sample c_S is directly derived from the relation $k=\rho c\alpha$, where ρ is the mass density, valid for a stationary state. The values of k_S and c_S found via this analysis are also shown in Table I.

Our value of thermal conductivity for untreated PEEK sample differs from that given by the PEEK film manufacturer by 28% (manufacturer value: 0.25 W/m K). Likewise, the specific heat difference was 10% (manufacturer value: 1.45 kJ/kg K). We believe that these differences can be explained by variations in the production process leading to structural and orientational differences between films.[1]

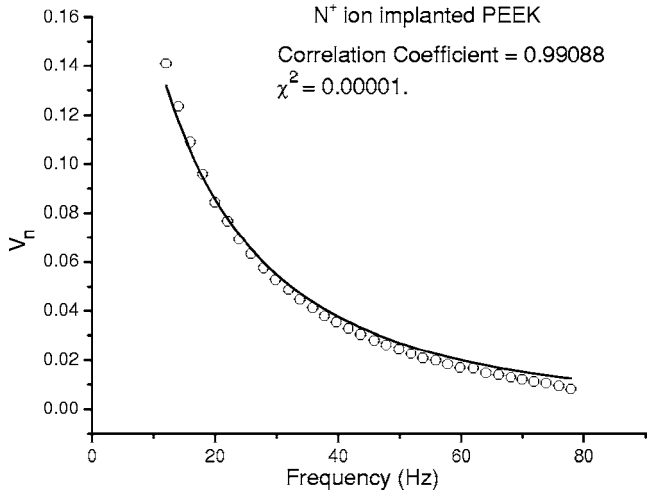

FIG. 6. Experimental points (dots) and line of best fit [Eq. (4)] for the PPE normalized voltage of the N^+ implanted PEEK film as a function of the chopping frequency of the input Xe lamp irradiation using the monochromator fixed at 340 nm.

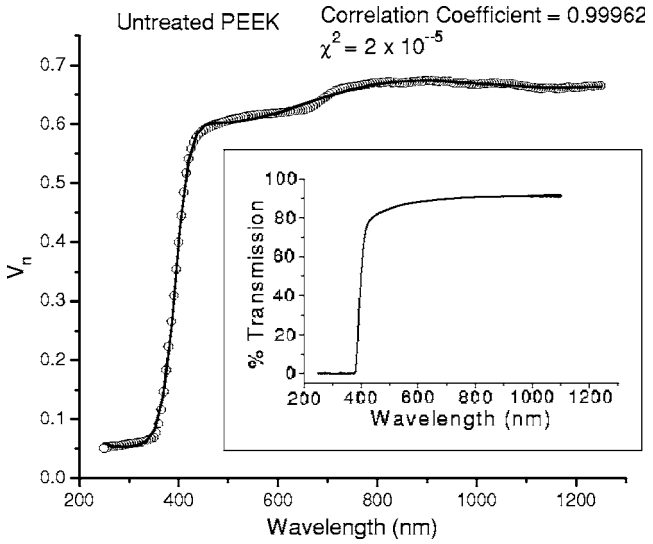

FIG. 7. PPE V_n spectrum as a function of wavelength for the untreated PEEK film at 20 Hz chopping frequency. The dots represent experimental results and the full line represents the fit [Eq. (3)]. The inset shows the conventional UV–Vis–near IR optical transmission spectrum of untreated PEEK film.

Figures 7 and 8 show PPE V_n and F_n spectra as a function of wavelength for the untreated PEEK sample at 20 Hz chopping frequency. The wavelength range was 250–1250 nm. The inset of Fig. 7 shows the conventional UV–Vis–near IR optical transmission spectrum of untreated PEEK film. The PPE signal follows qualitatively the optical transmission spectrum of the material (i.e., is transmission-like as predicted), and saturated for wavelengths below about 350 nm. The signal amplitude increases dramatically in the region $360<\lambda<430$ nm consistent with the primary gap of the polymer ($n-\pi^*$ of the ketone[3]). At wavelengths >430 nm the UV–Vis optical spectrum is flat and featureless. However, the PPE spectrum shows a second gaplike feature between 660 and 730 nm, which we attribute to a low level of impurity in the polymer or more likely a low energy $\pi-\pi^*$ transition arising from the aromatic moieties.[3] The

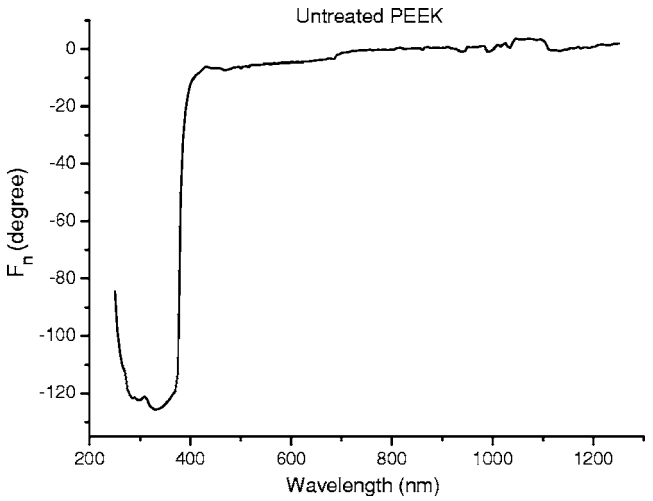

FIG. 8. PPE F_n spectrum as a function of wavelength of the untreated PEEK film at 20 Hz chopping frequency.

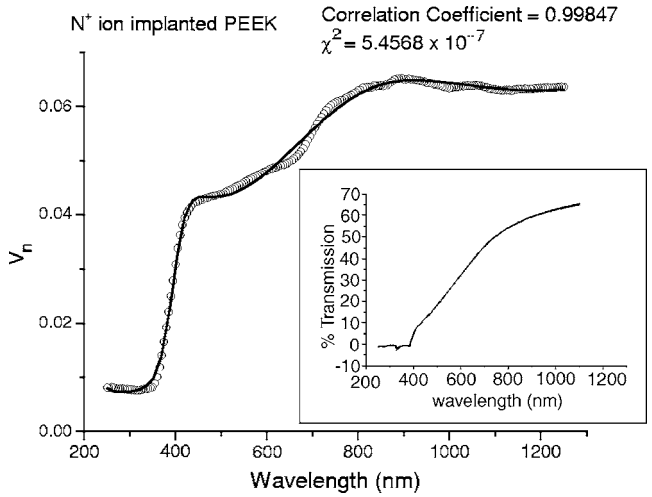

FIG. 9. PPE V_n spectrum as a function of wavelength of the N^+ implanted PEEK film at 20 Hz chopping frequency. The inset shows the conventional UV–Vis–near IR optical transmission spectrum of the N^+ implanted PEEK film.

absence of the feature in the transmission spectrum is an indication of how much more sensitive PPS techniques are than a simple optical measurement.

Figures 9 and 10 show PPE V_n and F_n spectra as a function of wavelength obtained for N^+ ion implanted PEEK (treated face in contact with the pyroelectric sensor) at 20 Hz chopping frequency. Once again, the spectra appear transmissionlike as expected at this chopping frequency. The inset of Fig. 9 shows the conventional UV–Vis–near IR optical transmission spectrum of N^+ implanted PEEK film. The major difference in the V_n spectrum compared to Fig. 7 is seen in the region between 430 and 730 nm. The intensity is significantly reduced in the ion implanted sample, and the second gaplike feature between 660 and 730 nm is very pronounced. In real terms, this indicates that significant absorption of the probe is occurring below 730 nm. We attribute this to the material of the implant region since one of the major effects of ion implantation in polymers is to increase the aromaticity in a graphitization process.[2] Once

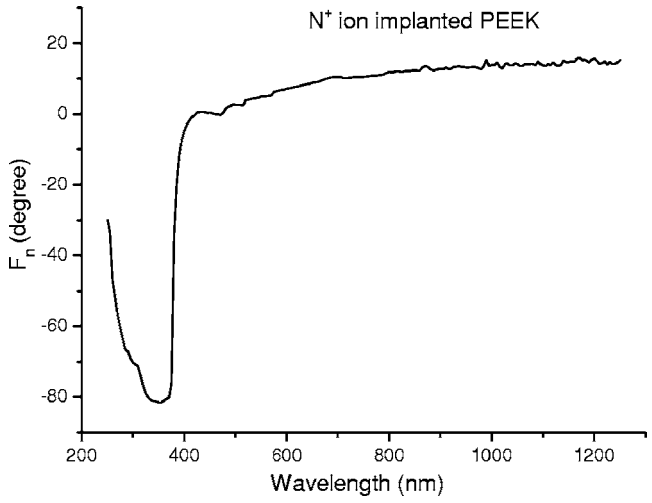

FIG. 10. PPE F_n spectrum as a function of wavelength of the N^+ implanted PEEK film at 20 Hz chopping frequency.

again, the simple optical transmission spectrum does not contain the detailed information of the PPE spectrum, which allows us to assign an optical gap to the ion implanted material of ~730 nm.

The continuous lines fitted to the PPE spectra of Figs. 7 and 9 were obtained from Eq. (3), obeying the thermally thick and optically opaque conditions of the pyroelectric detector. The absorption $\beta_s(\lambda)$ function was represented by two Gaussian functions (the minimum required), centered at 284 and 492 nm, which fitted well to the UV–Vis–near IR transmission spectrum for the untreated and N^+ implanted PEEK samples (see the insets of Figs. 7 and 9). The thermal quantities α_S and k_S obtained previously were used as fixed parameters here and the adjusted values were the intensity, the linewidth, and the center of the Gaussian functions. The flat plateau above 730 nm and the small shoulder observed in the experimental $V_n(\lambda)$ spectrum at ~1050 nm in Fig. 7 and the small signal decrease above 880 nm in Fig. 9 are only reproduced if a third Gaussian centered at 1450 nm is added to the $\beta_s(\lambda)$ function; otherwise, above 730 nm in Fig. 7 and above 880 nm in Fig. 9, a signal increase is always obtained without a flat plateau. For the untreated PEEK film (Fig. 7), the intensity of this third Gaussian is three orders of magnitude smaller than that at 284 nm and one order of magnitude smaller than that at 492 nm. It is therefore unsurprisingly not evident in the conventional optical spectrum. For the N^+ PEEK film (Fig. 9), the intensity of this third Gaussian is two orders of magnitude smaller than that at 284 nm and only 40% smaller than that at 492 nm. It is therefore observed as a shoulder at 492 nm and a long tail towards the infrared in conventional UV–Vis–near IR spectrum (see inset of Fig. 9). Despite the fact that these second and third absorption peaks are much smaller than that at 284 nm, it is surprising that such a small fraction of absorbed energy causes a relatively high nonradiative conversion energy and hence PPE signal. This fact shows the power of the PPE technique over the others conventionally used for studying these types of materials.

B. Depth profile analysis of ion implanted PEEK films using PAS

PA spectra were obtained in the $250 < \lambda < 1250$ nm wavelength range. For each PAS spectrum in that region, we used a discrete number of chopper frequencies between 20 and 3500 Hz. Table II presents the thermal diffusion lengths calculated using Eq. (7) at each chopping frequency for the untreated and the N^+ ion implanted PEEK films. As can be seen from this table, for all frequencies, the samples were thermally thick; that is, the thermal diffusion lengths of the samples were smaller than the thickness of the films. However, we know that the PA signal arises from deep within the sample to the external surface (into the illumination direction). Thus for higher frequencies, the PA signal corresponds to profiles closer to the external surface of the films.

Figures 11 and 12 show the spectra for the untreated PEEK sample and for the N^+ implanted PEEK, respectively, at lower chopping frequencies. Figure 13 shows the spectra obtained for the implanted sample at higher chopping fre-

TABLE II. Thermal diffusion lengths calculated using Eq. (7) at each chopping frequency of the PEEK samples.

	μ_S (μm)		
Frequency (Hz)	Untreated PEEK	N^+ ion implanted PEEK (untreated face in contact with PVDF)	N^+ ion implanted PEEK (treated face in contact with PVDF)
20	55	56	63
400	12	13	14
800	8.7	8.9	10
1500	6.3	6.5	7.3
2000	5.5	5.6	6.3
3000	4.5	4.6	5.2

quencies, repeating the frequency at 800 Hz for comparison. PA spectra always present absorptionlike behavior. Note that the highest frequency spectra (lowest signal-to-noise ratio) contain a number of lamp features between 800 and 1100 nm, which could not be removed through normalization or smoothing. From the spectra of Fig. 11, we can conclude that the untreated PEEK sample presents the primary gap between 295 and 400 nm, as shown in the 20 Hz spectrum. The PA signal above a wavelength of 1000 nm, as shown in the 800 Hz spectrum, represents a greater absorption near the surface of the film since the sampling depth decreases as the chopping frequency increases. This behavior is seen with the implanted PEEK sample at higher frequencies as shown in Figs. 12 and 13. Hence it is not related to ion implanted process.

Figures 12 and 13 show that the N^+ implanted PEEK sample has another broad absorption band starting at ~460 nm and extending to the near infrared region, and being more pronounced for higher frequencies. An explanation for the behavior of these spectra can be the fact that the thermal diffusion length decreases as chopper frequency increases, i.e., the PA signal is due to the heat produced from shallower regions in the sample. The effect of the nonimplanted bulk region is gradually diminished as the chopper frequency is increased, giving a better representation of the properties of the thin implanted layer. The band beginning at ~460 nm we believe is therefore related to N^+ ion implantation since the untreated PEEK does not show this feature (Fig. 11). This assertion agrees with the PPE observations of a second gaplike feature extending into the near IR in the transmissionlike spectra of the N^+ ion implanted films. In order to further confirm this hypothesis, we performed a PA spectral subtraction, i.e., the N^+ ion implanted PEEK PA signal minus the untreated PEEK PA signal. The goal here was to extract the contribution of the untreated PEEK signal from the N^+ implanted PEEK spectrum. In order to do this, we used a multiplication factor so that the resulting spectrum was always positive over the entire wavelength range. Figure 14 shows the resulting subtraction where the multiplication factor was 0.83, i.e., the untreated PEEK spectrum was multiplied by this factor before the subtraction. The inset shows the conventional UV–Vis–near IR optical absorption differ-

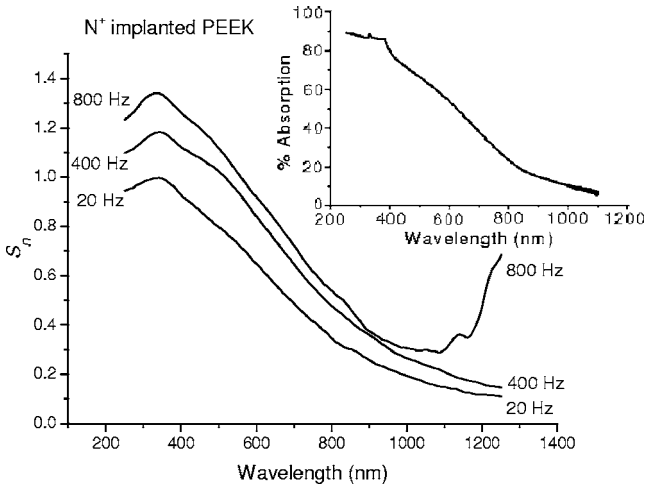

FIG. 12. PA spectra of the N^+ implanted PEEK film in various lower chopping modulation frequencies. The inset shows the conventional UV–Vis–near IR optical absorption spectrum of N^+ implanted PEEK film.

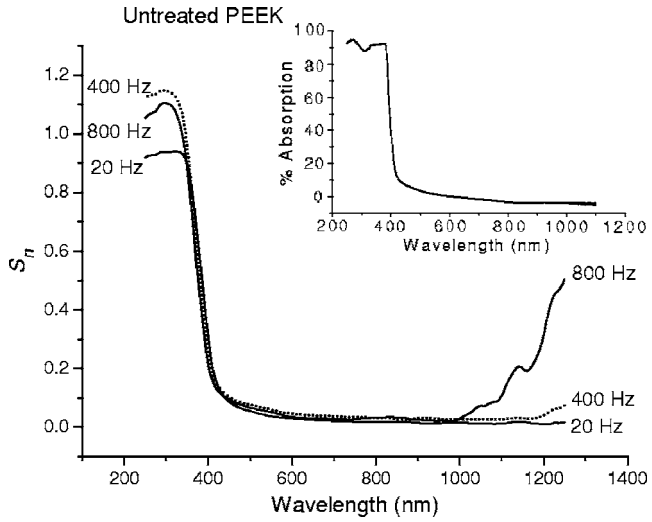

FIG. 11. PA spectra of untreated PEEK film in various lower chopping modulation frequencies. The inset shows the conventional UV–Vis–near IR optical absorption spectrum of untreated PEEK film.

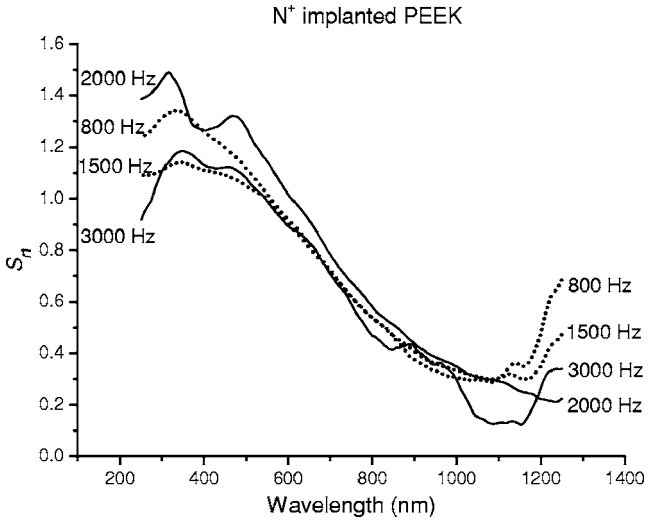

FIG. 13. PA spectra of the N^+ implanted PEEK film in various higher chopper modulation frequencies including previous 800 Hz frequency for comparison.

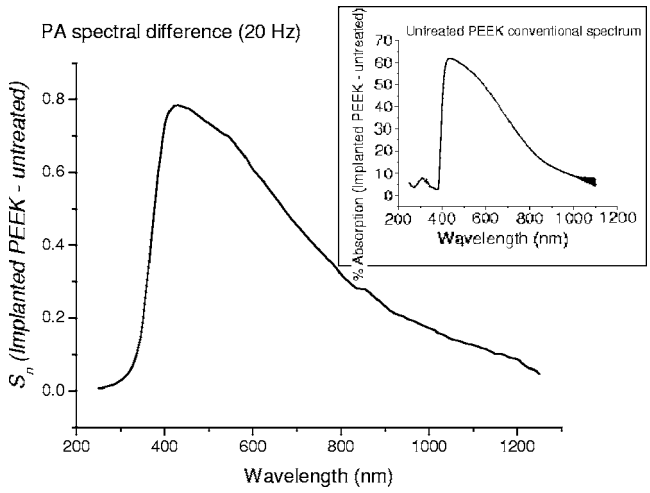

FIG. 14. PA spectral difference for N^+ implanted PEEK and untreated PEEK films corresponding to 20 Hz chopping frequency of Figs. 10 and 11. The inset shows the conventional UV–Vis–near IR optical absorption difference spectrum (% absorption of N^+ implanted film minus % absorption of untreated PEEK).

ence spectrum, that is, % absorption of the implanted PEEK film minus % absorption of untreated PEEK multiplied by 0.83. Thus we can see the broad absorption band beginning at around 450 nm extending into the near-IR region in both PA and conventional spectra. As suggested earlier, this broad absorption band could be due to increased conjugation and aromaticity of the carbon bonds by ion implantation (the aforementioned graphitization), resulting in a lowering of the band gap energy.[3] Hence, the PPE, PA, and depth profiling analyses are consistent with the formation of impurity bands within the band gap of PEEK due to ion implantation.

VI. CONCLUSIONS

In this article we have shown that the photothermal techniques (PPES and PAS) are powerful tools for studying the thermal and optical properties of PEEK films. Our results for the untreated PEEK agree reasonably with the manufacturers' reported values, and both the PPE and PAS spectra agree extremely well with the measured UV–Vis–near IR optical transmission and absorption. We observed and quantified significant changes in the optical and thermal properties of the PEEK films after implantation. These changes were even evident considering that the implant region is much thinner than the total film thickness. The most striking feature of the study was the emergence of a lower energy second optical gap (seen as a broad absorption beginning at ~490 nm and extending into the near IR in the ion implanted samples). This absorption was further qualified using PAS depth profiling. We attribute this absorption to increased conjugation and aromaticity in the implant region. This "graphitization process" has been observed using x-ray photoelectron spectroscopy surface analysis,[2] and we believe this to be the reason why the electrical conductivity of ion implanted PEEK is orders of magnitude larger than the native material. Our results have implications for the design and realization of optical and electrical devices and structures based on ion implanted polymers. For example, the increased specific heat capacity and thermal conductivity of the ion implanted sample, and additionally, its increased optical absorption in the near IR mean that effective, low cost near-IR bolometers could be realized in these materials. Additionally, PPS techniques appear to be effective and sensitive tools in monitoring the effects of implantation in polymers—a fact which could be used to optimize material properties and enhance device performance.

ACKNOWLEDGMENTS

This work was partially sponsored by FAPEMIG/MG/Brazil, by the Australian Research Council (DP0345309), by the Australian Institute of Nuclear Science and Engineering, and by the Missouri State University Center for Applied Science and Engineering.

[1] C. L. Choy, K. W. Kwok, W. P. Leung, and F. P. Lau, J. Polym. Sci., Part B: Polym. Phys. **32**, 1389 (1994).
[2] E. Tavenner, P. Meredith, B. Wood, M. Curry, and R. Giedd, Synth. Met. **145**, 183 (2004).
[3] R. C. Powles, D. R. McKenzie, N. Fujisawa, and D. G. McCulloch, Diamond Relat. Mater. **14**, 1577 (2005).
[4] G. R. Rao, E. H. Lee, and L. K. Mansur, Wear **174**, 103 (1994).
[5] S. Kim, K. Lee, and Y. Seo, Langmuir **20**, 157 (2004).
[6] J. Comyn, L. Mascia, G. Xiao, and B. M. Parker, Int. J. Adhes. Adhes. **16**, 97 (1996).
[7] A. Macková, V. Havránek, V. Svorcík, N. Djourelov, and T. Suzuki, Nucl. Instrum. Methods Phys. Res. B **240**, 245 (2005).
[8] D. R. McKenzie, K. Newton-McGee, P. Ruch, M. M. Bilek, and B. K. Gan, Surf. Coat. Technol. **186**, 239 (2004).
[9] V. Svorcík, K. Proková, V. Rybka, J. Vacík, V. Hnatowicz, and Y. Kobayashi, Mater. Lett. **36**, 128 (1998).
[10] A. C. Tam and Y. H. Wong, Appl. Phys. Lett. **36**, 471 (1980).
[11] J. C. Murphy and L. C. Aamodt, Appl. Phys. Lett. **38**, 196 (1981).
[12] H. Coufal, Appl. Phys. Lett. **44**, 59 (1984).
[13] A. Mandelis, Chem. Phys. Lett. **108**, 388 (1984).
[14] A. Rosencwaig, *Photoacoustics and Photoacoustic Spectroscopy* (Wiley, New York, 1980).
[15] A. Mandelis and M. M. Zver J. Appl. Phys. **57**, 4421 (1985).
[16] J. E. de Albuquerque, W. L. B. Melo, and R. M. Faria, J. Polym. Sci., Part B: Polym. Phys. **38**, 1294 (2000).
[17] J. E. de Albuquerque, W. L. B. Melo, and R. M. Faria, Mol. Cryst. Liq. Cryst. Sci. Technol., Sect. A **374**, 379 (2002).
[18] J. E. de Albuquerque, W. L. B. Melo, and R. M. Faria, Rev. Sci. Instrum. **74**, 306 (2003).
[19] W. L. B. Melo, A. Pawlicka, R. Sanches, S. Mascarenhas, and R. M. Faria, J. Appl. Phys. **74**, 979 (1993).
[20] J. E. de Albuquerque, D. T. Balogh, and R. M. Faria, J. Phys. IV **125**, 63 (2005).
[21] J. E. de Albuquerque, P. M. S. de Oliveira, and S. O. Ferreira, J. Phys. IV **125**, 169 (2005).
[22] J. E. de Albuquerque, C. Giacomantonio, A. G. White, and P. Meredith, Appl. Phys. Lett. **87**, 061920 (2005).
[23] J. E. de Albuquerque, C. Giacomantonio, A. G. White, and P. Meredith, Eur. Biophys. J. **35**, 190 (2006).
[24] A. Mandelis, F. Boroumand, H. Solka, J. Highfield, and H. Van Den Bergh, Appl. Spectrosc. **44**, 132 (1990).